

Diagnosing Quantum Many-body Chaos in Non-Hermitian Quantum Spin Chain via Krylov Complexity

Yijia Zhou,¹ Wei Xia,² Lin Li,³ and Weibin Li⁴

¹Shanghai Qi Zhi Institute, Shanghai 200232, China

²Department of Physics, The Chinese University of Hong Kong, Shatin, New Territories, Hong Kong, China

³MOE Key Laboratory of Fundamental Physical Quantities Measurement, Hubei Key Laboratory of Gravitation and Quantum Physics, PGMF, Institute for Quantum Science and Engineering, School of Physics, Huazhong University of Science and Technology, Wuhan 430074, China

⁴School of Physics and Astronomy, and Centre for the Mathematics and Theoretical Physics of Quantum Non-equilibrium Systems, The University of Nottingham, Nottingham NG7 2RD, United Kingdom

(Dated: January 28, 2025)

We investigate the phase transitions from chaotic to non-chaotic dynamics in a quantum spin chain with a local non-Hermitian disorder, which can be realized with a Rydberg atom array setting. As the disorder strength increases, the emergence of non-chaotic dynamics is qualitatively captured through the suppressed growth of Krylov complexity, and quantitatively identified through the reciprocity breaking of Krylov space. We further find that the localization in Krylov space generates another transition in the weak disorder regime, suggesting a weak ergodicity breaking. Our results closely align with conventional methods, such as the entanglement entropy and complex level spacing statistics, and pave the way to explore non-Hermitian phase transitions using Krylov complexity and associated metrics.

Introduction.— Diagnosis of chaos emerging in quantum systems attracts a growing interest, with a variety of measures including Lyapunov exponents [1–3], out-of-time-order correlations [4–6], Loschmidt echo [7–9], as well as spectral characteristics revealed through level spacing distributions [10–14] and spectral form factors [15–17]. Recently, Krylov complexity has emerged as an innovative approach to the study of quantum chaos [18–33]. Krylov complexity quantifies the spreading of quantum operators [18] or states [20] in Krylov space, capturing key features of the underlying dynamics.

A pivotal insight in this field is the operator growth hypothesis [18], which suggests that information scrambling and chaos can be identified by observing exponential growth in Krylov complexity at early times. The exponential growth is attributed to the linearity of Lanczos coefficients, which govern the tunneling rates in Krylov space. In contrast, another hypothesis focuses on the long-term dynamics and proposes a Tsallis q -log behavior of the Lanczos coefficients throughout the entire Krylov space [24, 32], where chaos can be signified by the linear growth in complexity at intermediate times, followed by a peak before saturation [20, 24, 27]. Additionally, the fluctuation in Lanczos coefficients, known as Krylov variance, has been shown to correlate with the delocalization of the Krylov wave function and, consequently, with ergodic behaviors [19, 21, 25, 28, 29, 33]. Despite extensive investigations in the Hermitian regime, challenges emerge when extending to open quantum systems. While Krylov complexity appears to be significantly reduced under dissipation [34–39], the Lanczos coefficients deviate from the established hypotheses for Hermitian systems, particularly when the absence of Hermiticity of

Krylov space is overlooked. Furthermore, the critical behavior and universal properties near phase transitions in open systems remain largely unexplored.

In this work, we investigate Krylov complexity of a non-Hermitian XY model with random local gain and loss. We show that the evolution of Krylov wave functions and complexity growth are indicative of phase transitions of quantum chaos. Through a closer examination of Lanczos coefficients, we uncover that the Krylov vari-

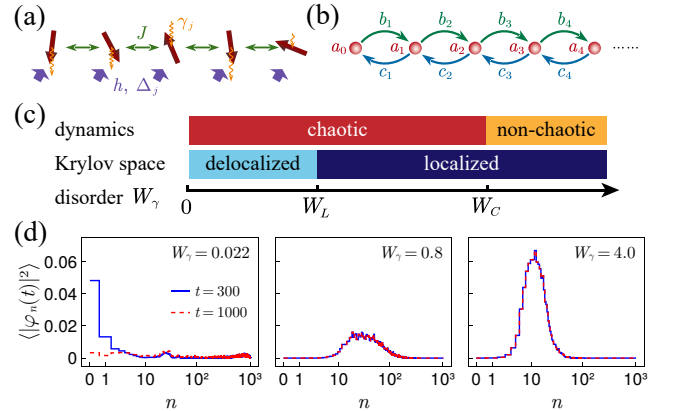


FIG. 1. (a) Disordered non-Hermitian XY model, with XY coupling J , transverse field h , site-dependent detuning $\Delta_j \in [-W_\Delta, W_\Delta]$, and dissipation $\gamma_j \in [-W_\gamma, W_\gamma]$. (b) Tunneling rates b_j and c_j are not conjugate for non-Hermitian systems. (c) Sketch of the phase diagram with increasing W_γ . (d) Krylov wave functions in chaotic regimes with delocalized (left) and localized (middle) profiles, and non-chaotic (right) regimes, at mid-term $t = 300$ (solid blue) and long-term $t = 1000$ (dashed red). See text for details.

ance elucidates critical points and universal features for localization of Krylov wave function which indicates a weak ergodicity breaking. We introduce a metric of reciprocity to underscore the suppression of quantum chaos, where the onset of non-reciprocity marks the corresponding critical point. The critical points determined using our method are quantitatively consistent with established metrics, including entanglement entropy variance [40, 41] and complex level spacing statistics [12–14]. Our framework is also applicable to other ergodicity-breaking phenomena, including many-body localization [21, 42], quantum scars [43], and Hilbert space fragmentation [44], and holds potential for extensions into machine learning applications [45]. The non-Hermitian XY model can be realized with Rydberg atom array quantum simulators. Our work thus opens avenues to experimentally explore complexities with observables such as Loschmidt echo [7, 46].

Model.— We study a one-dimensional disordered XY spin chain under both transverse and longitudinal fields, as depicted in Fig. 1(a). The Hamiltonian is given by

$$H = \sum_{j=1}^{L-1} J (\hat{\sigma}_j^x \hat{\sigma}_{j+1}^x + \hat{\sigma}_j^y \hat{\sigma}_{j+1}^y) + \sum_{j=1}^L h \hat{\sigma}_j^x + \mathcal{D}_j \hat{\sigma}_j^z, \quad (1)$$

where $\hat{\sigma}_j^x$, $\hat{\sigma}_j^y$, $\hat{\sigma}_j^z$ are Pauli matrices acting on the j -th site. The longitudinal field is random and complex, $\mathcal{D}_j = \Delta_j + i\gamma_j$, where the real part Δ_j and imaginary part γ_j give the detuning, and the gain or loss, respectively. The parameters Δ_j and γ_j are independently and uniformly distributed within $[-W_\Delta, W_\Delta]$ and $[-W_\gamma, W_\gamma]$, correspondingly. In the following calculations, we scale the Hamiltonian with the XY interaction strength J . To explore the non-Hermitian effects, we vary W_γ while fixing $h = 0.5$ and $W_\Delta = 1$ throughout the work. The model can be realized with Rydberg atom arrays, which will be discussed later.

In the Krylov space, the dynamics are mapped to a single-particle tight-binding model [see Fig. 1(b)]. The non-Hermitian Hamiltonian displays vastly different dynamics as the disorder strength W_γ increases. Specifically, two phase transitions are observed, where a suppression of spreading within finite Krylov subspace takes place at $W_\gamma = W_L \approx 0.0351$ revealing a localization feature, and a transition from chaotic to non-chaotic dynamics at $W_\gamma = W_C \approx 1.647$. The phase diagram is depicted in Fig. 1(c). These phases can be captured by the spreading of the Krylov wave function, illustrated in Fig. 1(d) [see Supplemental Materials (SM) for more examples]. For $W_\gamma < W_L$, the Krylov wave function is fully delocalized across the entire Krylov space at late times ($t = 1000$). For $W_\gamma > W_L$, conversely, a weak breaking of ergodicity may be indicated by the localized Krylov wave function with exponentially small occupation for $n \gtrsim \mathcal{O}(L^2)$. In the non-chaotic regime, $W_\gamma < W_C$, the wave function is further confined below $n \lesssim \mathcal{O}(L)$. We

also observe prethermal behavior in the Krylov delocalized regime, where the wave function is confined near $n \approx 0$ at mid-term times ($t = 300$), contrasting with other phases. Krylov complexity and Lanczos coefficients capture critical behaviors around the phase transition points. This allows us to determine the critical points through a number of measures, which will be discussed in detail in the following.

Krylov complexity.— The mathematical framework for representing quantum models in Krylov space involves a tridiagonalization process [47]. Krylov space is constructed by iteratively applying the Hamiltonian to an initial state vector and orthogonalizing it against the preceding basis vectors. This process is efficiently implemented using the bi-Lanczos algorithm, which is capable of dealing with non-Hermitian systems [36–38]. In Krylov space, the evolution of the quantum system is encapsulated as an effective single-particle tight-binding model on a semi-infinite chain [18]. The Krylov wave function φ_n is governed by the discrete equation (see SM for details),

$$i\dot{\varphi}_n = b_n \varphi_{n-1} + a_n \varphi_n + c_{n+1} \varphi_{n+1}, \quad (2)$$

where φ_n represents the distribution over the Krylov space. The Lanczos coefficients b_n and c_n are generally not complex conjugates, due to the non-Hermiticity of the Hamiltonian. The initial state is $\varphi_0 = 1$ and $\varphi_n = 0$ for $n > 0$.

Krylov complexity quantifies the spreading of the Krylov wave function by its *center of mass*, defined as

$$C_K = \sum_n n |\varphi_n(t)|^2. \quad (3)$$

The growth of Krylov complexity is a rich, multistage phenomenon. Figures 2(a1-a3) illustrate the complexity growth for system sizes $L = 6, 8,$ and 10 with the initial state $|\psi_0\rangle = |+\rangle^{\otimes L}$, where $|+\rangle = (|\uparrow\rangle + |\downarrow\rangle)/\sqrt{2}$. In case of Hermitian systems ($W_\gamma = 0$), the Krylov complexity typically shows generic quadratic-linear-peak-saturate shape, reminiscent of the slope-dip-ramp-plateau profile of the spectral form factor [24]. In our non-Hermitian spin chain model, we find distinctive features beyond these trends, indicating Krylov localization and chaos-non-chaos transition as W_γ increases.

The short-term growth of the Krylov complexity is universally quadratic, $C_K(t) \sim (1 + W_\gamma^2)t^2$ (see SM). The absence of exponential growth suggests a deviation from the operator growth hypothesis, as also corroborated by the nonlinear behavior of Lanczos coefficients [Fig. 2(b1-b4)]. Thus, it precludes chaos diagnosis using the early time dynamics in our model.

On the intermediate time scale, the Krylov complexity grows nonlinearly, deviating from the linear growth associated with spectral rigidity reported in previous studies [24]. Notably, for $W_\gamma < W_C$, C_K is bounded by a linear envelope, and its long-term saturation value increases

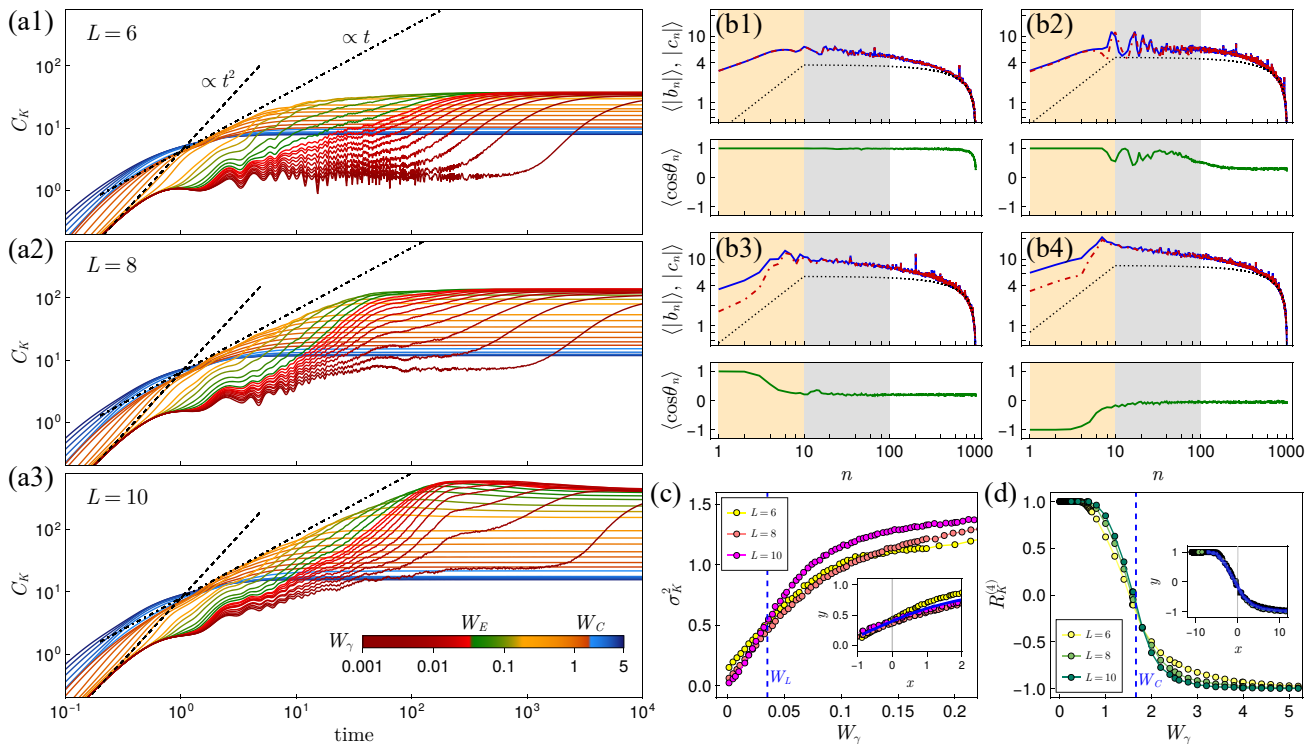


FIG. 2. (a) Krylov complexity growth. With $W_\Delta = 0.5$, W_γ varies from 0.001 to 5 across system sizes (a1) $L = 6$, (a2) $L = 8$, and (a3) $L = 10$. Dashed lines are the quadratic ($\sim t^2$) and dash-dot lines the linear ($\sim t$) trends, respectively. (b) Lanczos coefficients for $L = 10$ and $W_\gamma =$ (b1) 0.0118, (b2) 0.2, (b3) 1.0, and (b4) 3.0. Upper panels show $\langle |b_n| \rangle$ (solid blue) and $\langle |c_n| \rangle$ (dashed red), with dotted lines representing $\sim n$ for $n < L$, and $\sim \sqrt{1 - n/2^L}$ for $n > L$. Lower panels show $\langle \cos \theta_n \rangle$. (c) The Krylov variance given by Eq. (4), and the inset is the finite-size scaling, from which we obtain $W_L = 0.0351$. (d) Krylov reciprocity given by Eq. (5). The inset is the finite-size scaling yielding $W_C = 1.647$. Simulations are sampled and averaged over 1000, 600, and 400 trajectories for $L = 6, 8$, and 10, respectively.

as W_γ decreases. These phenomena indicate that chaos suppression correlates with confined spreading of Krylov wave function [Fig. 1(d)]. In chaotic regimes, the Krylov wave functions extend beyond the system size, as a result of the involvement of many excited states. Ref. [24] suggests a linear ramp of the Krylov complexity due to the Lanczos coefficients following $b_n \propto \sqrt{1 - n/2^L}$, which is a special case of Tsallis q -log statistics with $q = 0$ [32]. In contrast, we find $q > 0$ in our results (see SM), as shown in Figs. 2(b1-b4). The mid-term ramp, on the other hand, indicates spectral rigidity as it is constrained by a linear envelope [Fig. 2(a)].

In the Krylov delocalized regime ($W_\gamma < W_L$), the Krylov complexity shows prethermal behaviors, where oscillations and a low saturation plateau emerge before a rapid increase to higher values. This behavior stems from dynamics confined to a small Krylov subspace due to small overlaps between the initial state and eigenstates with large imaginary components. For example, for $W_\gamma = 0.022$ and at $t = 300$, the system forms a prethermal state where the Krylov wave function is localized at $n < \mathcal{O}(L)$ [Fig. 1(d)]. At longer times $t \gtrsim 10^3$, C_K saturates as the Krylov wave function completely de-

localizes. As system size increases, C_K exhibits damped oscillations, and the saturation time grows significantly.

Krylov variance and reciprocity.— Beyond the growth of C_K , a metric known as Krylov variance [22] has been proposed to measure the fluctuation of the Lanczos coefficients, which characterizes the localization of the Krylov wave function as an analogue to Anderson localization [48]. In Hermitian systems, the Krylov variance is defined as $\sigma_K^2 = \text{Var}\{\ln |b_{2n-1}/b_{2n}|\}$ [22]. Similarly, we define the variance of the non-Hermitian system by replacing b_n with $j_n = |b_n c_n|^{1/2}$, yielding

$$\sigma_K^2 = \text{Var} \left\{ \ln \frac{j_{2n-1}}{j_{2n}} \right\}, \quad n = 1, 2, 3, \dots \quad (4)$$

Figure 2(c) shows the Krylov variance first grows with increasing W_γ and saturates at larger W_γ . Through finite-size scaling, we find σ_K^2 can be universally fitted with function $y = \sigma_K^2 L^{-\beta}$ against $x = (W_\gamma - W_L)L^\alpha$ [see inset of Fig. 2(c)]. This allows us to identify a critical point, $W_L = 0.0351$, with exponents $\alpha = 1.816$ and $\beta = 0.112$. When $W_\gamma < W_L$, the Krylov variance is small, which results in the delocalization of the Krylov wave function [Fig. 1(d)]. When $W_\gamma > W_L$, the Krylov

wave function localizes in a finite region. Here, the system is still chaotic, as supported by the level repulsion (as discussed below). Yet, the localized Krylov wave function and hence the suppression of Krylov complexity emerge as a signature of ergodicity breaking [21, 29, 33].

In non-Hermitian systems, Lanczos coefficients b_n and c_n are not complex conjugates, violating the reciprocity of the Krylov space. To quantify this, we evaluate arguments of the Lanczos coefficients, $\theta_n = \arg(b_n c_n)$, such that $\cos \theta_n = 1$ represents reciprocal tunneling, and $\cos \theta_n = -1$ gives the maximally non-reciprocal tunneling, which is associated with rapid relaxation. Figures 2(b1-b4) show the profiles of $\cos \theta_n$ as W_γ increases. Specifically, for $W_\gamma < W_L$, the entire Krylov space remains reciprocal, supporting delocalization of the Krylov wave function. For $W_L < W_\gamma < W_C$, tunneling within $n < L$ is reciprocal, but a rapid relaxation occurs as the Krylov wave function spreads to $n > L$. For $W_\gamma > W_C$, the Krylov wave function rapidly relaxes within $n < L$, as the first few sites become maximally non-reciprocal.

To leverage the sign-flip behavior of $\cos \theta_n$, we introduce a parameterized metric,

$$R_K^{(d)} = \frac{1}{d} \sum_{n=1}^d \cos \theta_n, \quad (5)$$

which is insensitive to the choice of d for a certain range smaller than L . We show this reciprocal metric in Fig. 2(d) for $d = 4$, and more examples in SM. For different L , $R_K^{(d)}$ collapses to $y = R_K^{(d)}$ with $x = (W_\gamma - W_C)L^\alpha$, yielding the mean critical point $W_C = 1.647$ and exponent $\alpha = 0.820$ for $d \in \{4, 5, 6\}$, with the relative deviation $< 1\%$. The universal scaling thus shows the transition from the chaotic to non-chaotic phases.

Entanglement entropy and level spacing.— To provide a comprehensive view of the aforementioned phase transitions, we bridge the findings from the Krylov complexity with conventional signatures of quantum chaos including entanglement entropy and complex level spacing. It is known that the chaos-non-chaos transition can be signified by the divergence of the variance of the bipartite entanglement entropy [40]. We show the standard deviation of the bipartite entanglement entropy, σ_S , in Fig. 3(a). A divergent peak is observed as $L \rightarrow \infty$. The data can be universally described by function $y = \sigma_S L^{-\beta}$ with respect to $x = (W_\gamma - W'_C)L^\alpha$ [inset of Fig. 3(a)]. This leads to the critical point $W'_C = 1.763$ with exponents $\alpha = 2.013$ and $\beta = 1.228$. Furthermore, a critical behavior at very small W_γ can be seen in Fig. 3(b). Using a similar scaling method, we identify the critical point $W'_L = 0.0409$ and exponents $\alpha = 1.514$ and $\beta = -0.054$. The critical points extracted from σ_S are similar to the ones of the Krylov complexity. In addition, we obtain a different critical point at $W^* = 3.236$ with the finite-size analysis of the entanglement entropy, S (see SM). This attributes to the transition to integrability as the

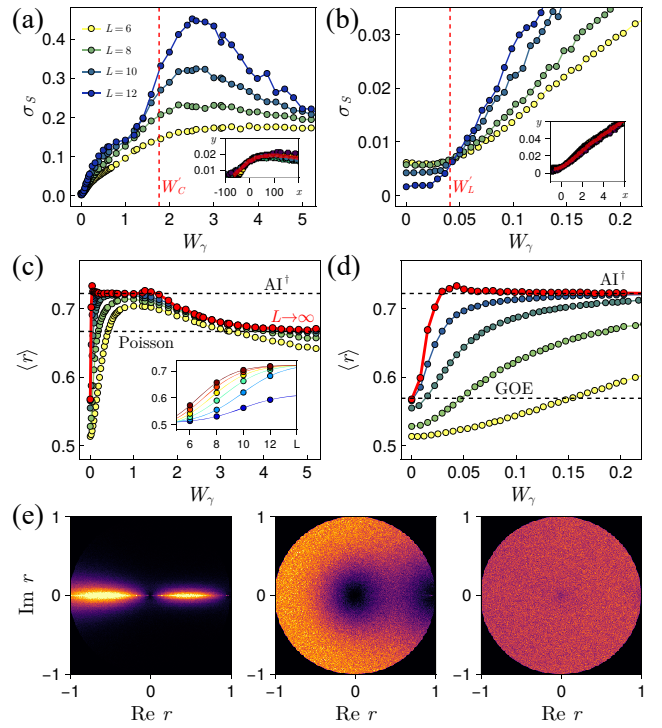


FIG. 3. (a) and (b) Standard deviation of bipartite entanglement entropy, σ_S , for different ranges of W_γ . The finite-size scaling [insets in (a) and (b)] yields critical points $W'_C = 1.763$ and $W'_L = 0.0409$. (c) and (d) Complex level spacing ratio for different ranges of W_γ . Dot lines (red) are the extrapolated values when $L \rightarrow \infty$. See examples shown in the inset of (c). (e) Distributions of complex level spacing ratios for $W_\gamma = 0.005, 0.8$, and 5.0 (from left to right), corresponding to GOE, AI^\dagger class, and 2D Poisson ensemble, respectively.

system is well described by product states when W_γ is sufficiently large.

Another widely recognized method to determine quantum chaos is the complex level spacing ratio (CSR), $r_j = (z_{j,\text{NN}} - z_j)/(z_{j,\text{NNN}} - z_j)$, where z_j is an eigenvalue of Hamiltonian (1), and $z_{j,\text{NN}}$ and $z_{j,\text{NNN}}$ are its nearest-neighbor and next-nearest-neighbor eigenvalues [12]. The mean absolute value of CSR, $\langle r \rangle = \int |r| P(r) dr$, is shown in Figs. 3(c,d). Increasing W_γ , the level statistics change from the Gaussian orthogonal ensemble (GOE) to AI^\dagger class, and then to the 2D Poisson ensemble [Fig. 3(e)]. To minimize the finite size effects, we extrapolate $\langle r \rangle_\infty$ in the limit $L \rightarrow \infty$ [red dots in Figs. 3(c,d)] [49]. As $W_\gamma \rightarrow 0$, $\langle r \rangle_\infty = 0.567$, consistent with $\langle r \rangle_{\text{GOE}} = 0.5689$ [11]. A plateau appears when $0.025 \lesssim W_\gamma \lesssim 1.6$, where $\langle r \rangle_\infty = 0.726(3)$, indicating that the system belongs to the AI^\dagger class, whose $\langle r \rangle_{\text{AI}^\dagger} = 0.7222$ [14]. Increasing W_γ from W'_C to W^* , the level statistics deviate from the AI^\dagger class and become the 2D Poisson ensemble. In this region, $\langle r \rangle_\infty = 0.6673(4)$, close to the 2D Poisson ensemble where $\langle r \rangle_{\text{Poi}(2\text{D})} = 2/3$ [12]. Therefore, the level statistics are consistent with the results of Krylov complexity.

Conclusions.— In conclusion, we have studied non-Hermitian quantum chaos in the disordered XY model, revealing two critical phase transitions including the chaotic-non-chaotic transition and Krylov localization. Through examining the Krylov complexity and Lanczos coefficients characterized by the Krylov variance and reciprocity, we identify the critical points and exponents of these phase transitions. Our results are corroborated by established measures including entanglement entropy and complex level spacings, which showcase the applicability of Krylov complexity and the associated measures in the study of quantum chaos. The sign-flip of Krylov reciprocity provides a quantitatively more precise criterion for chaos suppression than the entanglement entropy. Furthermore, we observe intricate chaotic behavior in non-Hermitian systems, where prethermalization may exist in the Krylov delocalized regime.

The non-Hermitian spin model can be realized in Rydberg atom arrays, where spin states are encoded by two Rydberg states [50]. The XY interactions correspond to the dipole-dipole interactions between the Rydberg states, and the dissipation can be induced by coupling the Rydberg states to low-lying electronic states [51]. Randomness of the local fields can be introduced by AC-Stark shifts with addressing lasers. In generic quantum simulators, non-Hermiticity can be realized through Sz.-Nagy dilation [52, 53] and linear combination of unitaries [54, 55]. Finally, to measure the Krylov complexity, it has been proposed to apply measurable bases for estimation [56], and the measure of Loschmidt echo is potentially related to the ergodicity breaking [Fig. 1(d)].

We are grateful to Dong-Ling Deng, Dong Yuan, Si Jiang, Chang Liu (SQZI), Chang Liu (NUS), Tianyi Yan, Xiaopeng Li, Xingze Qiu and Saud Ćindrak for fruitful discussions. Y.Z. acknowledges support from the Shanghai Qi Zhi Institute Innovation Program SQZ202317. W.X. acknowledges support from the National Natural Science Foundation of China/Hong Kong RGC Collaborative Research Scheme (Project CRS CUHK401/22) and New Cornerstone Science Foundation. L.L. acknowledges support from the National Key Research and Development Program of China (Grant No. 2021YFA1402003) and the National Natural Science Foundation of China (Grant Nos. 12374329 and U21A6006). W.L. acknowledges support from the EPSRC through Grant No. EP/W015641/1, the Going Global Partnerships Programme of the British Council (Contract No. IND/CONT/G/22-23/26), and the International Research Collaboration Fund of the University of Nottingham.

[1] H. A. Cerdeira, K. Furuya, and B. A. Huberman, Lyapunov Exponent for Quantum Dissipative Systems, *Phys. Rev. Lett.* **61**, 2511 (1988).

- [2] J. Chávez-Carlos, B. López-del-Carpio, M. A. Bastarrachea-Magnani, P. Stránský, S. Lerma-Hernández, L. F. Santos, and J. G. Hirsch, Quantum and Classical Lyapunov Exponents in Atom-Field Interaction Systems, *Phys. Rev. Lett.* **122**, 024101 (2019).
- [3] A. M. García-García, J. J. M. Verbaarschot, and J.-p. Zheng, Lyapunov exponent as a signature of dissipative many-body quantum chaos, *Phys. Rev. D* **110**, 086010 (2024).
- [4] M. Gärttner, J. G. Bohnet, A. Safavi-Naini, M. L. Wall, J. J. Bollinger, and A. M. Rey, Measuring out-of-time-order correlations and multiple quantum spectra in a trapped-ion quantum magnet, *Nat. Phys.* **13**, 781 (2017).
- [5] X. Chen, T. Zhou, D. A. Huse, and E. Fradkin, Out-of-time-order correlations in many-body localized and thermal phases, *Ann. Phys.* **529**, 1600332 (2017).
- [6] S. Xu and B. Swingle, Scrambling Dynamics and Out-of-Time-Ordered Correlators in Quantum Many-Body Systems, *PRX Quantum* **5**, 010201 (2024).
- [7] T. Gorin, T. Prosen, T. H. Seligman, and M. Žnidarič, Dynamics of Loschmidt echoes and fidelity decay, *Phys. Rep.* **435**, 33 (2006).
- [8] B. Yan, L. Cincio, and W. H. Zurek, Information Scrambling and Loschmidt Echo, *Phys. Rev. Lett.* **124**, 160603 (2020).
- [9] Y. Hasegawa, Irreversibility, Loschmidt echo, and thermodynamic uncertainty relation, *Phys. Rev. Lett.* **127**, 240602 (2021).
- [10] Y. Y. Atas, E. Bogomolny, O. Giraud, and G. Roux, Distribution of the Ratio of Consecutive Level Spacings in Random Matrix Ensembles, *Phys. Rev. Lett.* **110**, 084101 (2013).
- [11] S. C. L. Srivastava, A. Lakshminarayanan, S. Tomsovic, and A. Bäcker, Ordered level spacing probability densities, *J. Phys. A: Math. Theor.* **52**, 025101 (2019).
- [12] L. Sá, P. Ribeiro, and T. Prosen, Complex Spacing Ratios: A Signature of Dissipative Quantum Chaos, *Phys. Rev. X* **10**, 021019 (2020).
- [13] R. Hamazaki, K. Kawabata, N. Kura, and M. Ueda, Universality classes of non-Hermitian random matrices, *Phys. Rev. Res.* **2**, 023286 (2020).
- [14] A. M. García-García, L. Sá, and J. J. M. Verbaarschot, Symmetry Classification and Universality in Non-Hermitian Many-Body Quantum Chaos by the Sachdev-Ye-Kitaev Model, *Phys. Rev. X* **12**, 021040 (2022).
- [15] M. V. Berry, Semiclassical theory of spectral rigidity, *Proc. R. Soc. Lond., A. Math. Phys. Sci.* **400**, 229 (1985).
- [16] B. Bertini, P. Kos, and T. Prosen, Exact Spectral Form Factor in a Minimal Model of Many-Body Quantum Chaos, *Phys. Rev. Lett.* **121**, 264101 (2018).
- [17] H. Dong, P. Zhang, C. B. Dag, Y. Gao, N. Wang, J. Deng, X. Zhang, J. Chen, S. Xu, K. Wang, Y. Wu, C. Zhang, F. Jin, X. Zhu, A. Zhang, Y. Zou, Z. Tan, Z. Cui, Z. Zhu, F. Shen, T. Li, J. Zhong, Z. Bao, H. Li, Z. Wang, Q. Guo, C. Song, F. Liu, A. Chan, L. Ying, and H. Wang, Measuring Spectral Form Factor in Many-Body Chaotic and Localized Phases of Quantum Processors, *Phys. Rev. Lett.* **134**, 010402 (2025).
- [18] D. E. Parker, X. Cao, A. Avdoshkin, T. Scaffidi, and E. Altman, A universal operator growth hypothesis, *Phys. Rev. X* **9**, 041017 (2019).
- [19] A. Dymarsky and A. Gorsky, Quantum chaos as delo-

- calization in Krylov space, *Phys. Rev. B* **102**, 085137 (2020).
- [20] V. Balasubramanian, P. Caputa, J. Magan, and Q. Wu, Quantum chaos and the complexity of spread of states, *Phys. Rev. D* **106**, 046007 (2022).
- [21] F. Ballar Trigueros and C.-J. Lin, Krylov complexity of many-body localization: Operator localization in Krylov basis, *SciPost Phys.* **13**, 037 (2022).
- [22] E. Rabinovici, A. Sánchez-Garrido, R. Shir, and J. Sonner, Krylov localization and suppression of complexity, *J. High Energy Phys.* **2022** (3), 211.
- [23] E. Rabinovici, A. Sánchez-Garrido, R. Shir, and J. Sonner, Krylov complexity from integrability to chaos, *J. High Energy Phys.* **2022** (7), 151.
- [24] J. Erdmenger, S.-K. Jian, and Z.-Y. Xian, Universal chaotic dynamics from Krylov space, *J. High Energy Phys.* **2023** (8), 176.
- [25] K. Hashimoto, K. Murata, N. Tanahashi, and R. Watanabe, Krylov complexity and chaos in quantum mechanics, *J. High Energy Phys.* **2023** (11), 40.
- [26] B. L. Español and D. A. Wisniacki, Assessing the saturation of Krylov complexity as a measure of chaos, *Phys. Rev. E* **107**, 024217 (2023).
- [27] M. Baggioli, K.-B. Huh, H.-S. Jeong, K.-Y. Kim, and J. F. Pedraza, Krylov complexity as an order parameter for quantum chaotic-integrable transitions, [arXiv:2407.17054](https://arxiv.org/abs/2407.17054) (2024).
- [28] G. F. Scialchi, A. J. Roncaglia, and D. A. Wisniacki, Integrability-to-chaos transition through the Krylov approach for state evolution, *Phys. Rev. E* **109**, 054209 (2024).
- [29] H. G. Menzler and R. Jha, Krylov Delocalization/Localization across Ergodicity Breaking, *Phys. Rev. B* **110**, 125137 (2024).
- [30] H. A. Camargo, K.-B. Huh, V. Jahnke, H.-S. Jeong, K.-Y. Kim, and M. Nishida, Spread and Spectral Complexity in Quantum Spin Chains: From Integrability to Chaos, *J. High Energy Phys.* **2024** (8), 241.
- [31] L. Chen, B. Mu, H. Wang, and P. Zhang, Dissecting Quantum Many-body Chaos in the Krylov Space, [arXiv:2404.08207](https://arxiv.org/abs/2404.08207) (2024).
- [32] B. Bhattacharjee and P. Nandy, Krylov fractality and complexity in generic random matrix ensembles, [arXiv:2407.07399](https://arxiv.org/abs/2407.07399) (2024).
- [33] Z. Li and W. Fan, Statistical features of quantum chaos using the Krylov operator complexity, [arXiv:2411.18436](https://arxiv.org/abs/2411.18436) (2024).
- [34] A. Bhattacharya, P. Nandy, P. P. Nath, and H. Sahu, Operator growth and Krylov construction in dissipative open quantum systems, *J. High Energy Phys.* **2022** (12), 81.
- [35] C. Liu, H. Tang, and H. Zhai, Krylov complexity in open quantum systems, *Phys. Rev. Res.* **5**, 033085 (2023).
- [36] A. Bhattacharya, P. Nandy, P. P. Nath, and H. Sahu, On Krylov complexity in open systems: An approach via bi-Lanczos algorithm, *J. High Energy Phys.* **2023** (12), 66.
- [37] N. S. Srivatsa and C. Von Keyserlingk, Operator growth hypothesis in open quantum systems, *Phys. Rev. B* **109**, 125149 (2024).
- [38] E. Carolan, A. Kiely, S. Campbell, and S. Deffner, Operator growth and spread complexity in open quantum systems, *Europhys. Lett.* **147**, 38002 (2024).
- [39] A. Bhattacharya, P. P. Nath, and H. Sahu, Speed limits to the growth of Krylov complexity in open quantum systems, *Phys. Rev. D* **109**, L121902 (2024).
- [40] J. A. Kjäll, J. H. Bardarson, and F. Pollmann, Many-body localization in a disordered quantum ising chain, *Phys. Rev. Lett.* **113**, 107204 (2014).
- [41] R. Hamazaki, K. Kawabata, and M. Ueda, Non-hermitian many-body localization, *Phys. Rev. Lett.* **123**, 90603 (2019).
- [42] M. Ganguli and A. Jana, State Dependent Spread Complexity Dynamics in Many-Body Localization Transition, [arXiv:2409.02186](https://arxiv.org/abs/2409.02186) (2024).
- [43] B. Bhattacharjee, S. Sur, and P. Nandy, Probing quantum scars and weak ergodicity-breaking through quantum complexity, *Phys. Rev. B* **106**, 205150 (2022).
- [44] S. Balasubramanian, S. Gopalakrishnan, A. Khudorozhkov, and E. Lake, Glassy Word Problems: Ultraslow Relaxation, Hilbert Space Jamming, and Computational Complexity, *Phys. Rev. X* **14**, 021034 (2024).
- [45] S. Čindrak, L. Jaurigue, and K. Lüdige, Krylov Expressivity in Quantum Reservoir Computing and Quantum Extreme Learning, [arXiv:2409.12079](https://arxiv.org/abs/2409.12079) (2024).
- [46] S. Geier, A. Braemer, E. Braun, M. Müllenbach, T. Franz, M. Gärttner, G. Zürn, and M. Weidemüller, Time-reversal in a dipolar quantum many-body spin system, *Phys. Rev. Res.* **6**, 033197 (2024).
- [47] J. Liesen and Z. Strakoš, *Krylov Subspace Methods: Principles and Analysis*, 1st ed., Numerical Mathematics and Scientific Computation (Oxford University Press, Oxford, 2013).
- [48] L. Fleishman and D. C. Licciardello, Fluctuations and localization in one dimension, *J. Phys. C: Solid State Phys.* **10**, L125 (1977).
- [49] We assume the signatures of CSR for different system size read $\langle r \rangle = \langle r \rangle_\infty + \Delta r (1 + \exp[-a(L - L_0)])^{-1}$ where $\langle r \rangle_\infty$, Δr , a , L_0 are fitting parameters. The values of W_γ for the data in the inset are 0.01, 0.036, 0.064, 0.095, 0.126, and 0.158 (from blue to red).
- [50] S. De Léséleuc, V. Lienhard, P. Scholl, D. Barredo, S. Weber, N. Lang, H. P. Büchler, T. Lahaye, and A. Browaeys, Observation of a symmetry-protected topological phase of interacting bosons with Rydberg atoms, *Science* **365**, 775 (2019).
- [51] J. A. S. Lourenço, G. Higgins, C. Zhang, M. Henrich, and T. Macrì, Non-Hermitian dynamics and \mathcal{PT} -symmetry breaking in interacting mesoscopic Rydberg platforms, *Phys. Rev. A* **106**, 023309 (2022).
- [52] R. Sweke, I. Sinayskiy, D. Bernard, and F. Petruccione, Universal simulation of Markovian open quantum systems, *Phys. Rev. A* **91**, 062308 (2015).
- [53] Z. Hu, R. Xia, and S. Kais, A quantum algorithm for evolving open quantum dynamics on quantum computing devices, *Sci. Rep.* **10**, 3301 (2020).
- [54] A. M. Childs and N. Wiebe, Hamiltonian Simulation Using Linear Combinations of Unitary Operations, *Quantum Inf. Comput.* **12**, 0901 (2012).
- [55] A. W. Schlimgen, K. Head-Marsden, L. M. Sager, P. Narang, and D. A. Mazziotti, Quantum Simulation of Open Quantum Systems Using a Unitary Decomposition of Operators, *Phys. Rev. Lett.* **127**, 270503 (2021).
- [56] S. Čindrak, A. Paschke, L. Jaurigue, and K. Lüdige, Measurable Krylov spaces and eigenenergy count in quantum state dynamics, *J. High Energy Phys.* **2024** (10), 83.

Supplemental Materials for: Diagnosing Quantum Many-body Chaos in Non-Hermitian Quantum Spin Chain via Krylov Complexity

Yijia Zhou,¹ Wei Xia,² Lin Li,³ and Weibin Li⁴

¹*Shanghai Qi Zhi Institute, 41st Floor, AI Tower,
No. 701 Yunjin Road, Xuhui District, Shanghai, 200232, China*

²*Department of Physics, The Chinese University of Hong Kong, Shatin, New Territories, Hong Kong, China*

³*MOE Key Laboratory of Fundamental Physical Quantities Measurement,
Hubei Key Laboratory of Gravitation and Quantum Physics, PGMF,
Institute for Quantum Science and Engineering, School of Physics,
Huazhong University of Science and Technology, Wuhan 430074, China*

⁴*School of Physics and Astronomy, and Centre for the Mathematics
and Theoretical Physics of Quantum Non-equilibrium Systems,
The University of Nottingham, Nottingham NG7 2RD, United Kingdom*

(Dated: January 27, 2025)

KRYLOV SPACE AND BI-LANCZOS ALGORITHM

The study of Krylov complexity has its roots in solving Schrödinger equations, which starts with the temporal evolution of the wave function,

$$\psi(t) = e^{-iHt}\psi_0 = \sum_n \frac{(-it)^n}{n!} H^n \psi_0. \quad (S1)$$

In this context, the Hamiltonian H and the initial wave function ψ_0 spans a Krylov space,

$$\mathcal{K}(H, \psi_0) = \text{span}\{\psi_0, H\psi_0, H^2\psi_0, \dots\}. \quad (S2)$$

Contrasting with the Hermitian scenario, a non-Hermitian Hamiltonian generates a bi-orthogonal system, which includes an additional dual space,

$$\mathcal{K}^*(H, \psi_0) = \text{span}\{\psi_0, H^\dagger\psi_0, H^{\dagger 2}\psi_0, \dots\}. \quad (S3)$$

These spaces can be orthogonalized to yield two sets of vectors, $\text{span}\{p_0, p_1, p_2, \dots\}$ and $\text{span}\{q_0, q_1, q_2, \dots\}$, which fulfill the bi-orthogonality condition,

$$q_m^\dagger p_n = \delta_{mn}. \quad (S4)$$

It is noteworthy that the corresponding matrices $P = [p_0, p_1, p_2, \dots]$ and $Q = [q_0, q_1, q_2, \dots]$ are not unitary. Consequently, the Hamiltonian can be tridiagonalized through the relation,

$$T = Q^\dagger H P, \quad (S5)$$

with $Q^\dagger P = P Q^\dagger = I$ given that P and Q are both square and invertible.

This process can be numerically executed via the bi-Lanczos (two-sided Lanczos) iteration. To circumvent the breakdown issue, we have employed the complete reorthogonalization algorithm in this study, as shown in Algorithm 1. We note that there are also several more expeditious methods, such as selective and partial reorthogonalization [1–3].

With this methodology, the amplitude of the wave function within the Krylov space is defined by,

$$\varphi_n(t) = q_n^\dagger \psi(t). \quad (S6)$$

Subsequently, a three-term recurrence relation is derived from relation $HP = PT$,

$$H p_n = b_{n+1} p_{n+1} + a_n p_n + c_n p_{n-1}, \quad (S7)$$

where the coefficients b_n , a_n , c_n are the diagonal and sub-diagonal elements of the tridiagonal matrix T . This recurrence relation facilitates the temporal evolution of the coefficients $\varphi_n(t)$, akin to an effective tight-binding model,

$$i \frac{\partial}{\partial t} \varphi_n = b_n \varphi_{n-1} + a_n \varphi_n + c_{n+1} \varphi_{n+1}. \quad (S8)$$

We note that the Arnoldi iteration, also known as the modified Gram-Schmidt algorithm, can deal with more general forms of H with good numerical stability, albeit resulting in a more intricate recurrence relation, where the tridiagonal matrix T is replaced by a Hessenberg matrix.

Algorithm 1: Bi-Lanczos Algorithm with Complete Reorthogonalization

```

Input:  $H, \psi_0$ 
Output: Lanczos coefficients:  $\{a_n\}, \{b_n\}, \{c_n\}$ ; Krylov basis:  $\{p_n\}, \{q_n\}$ 
1  $b_0, c_0 \leftarrow 0, \quad p_0, q_0 \leftarrow \psi_0$  // Initialize
2 for  $n = 0$  to  $d - 2$  do //  $d = 2^L$  is the dimension of the Hilbert space and  $L$  is the system size
3    $p_{n+1}, q_{n+1} \leftarrow H p_n, H^\dagger q_n$ 
4    $a_n \leftarrow q_n^\dagger p_{n+1}$ 
5    $p_{n+1} \leftarrow p_{n+1} - a_n p_n - c_n p_{n-1}$  //  $p_{-1} = 0$ 
6    $q_{n+1} \leftarrow q_{n+1} - a_n^* q_n - b_n^* q_{n-1}$  //  $q_{-1} = 0$ 
7    $W \leftarrow [p_0, p_1, \dots, p_n][q_0, q_1, \dots, q_n]^\dagger$  // Complete reorthogonalization
8    $res \leftarrow 0$ 
9   while  $res < 0.707$  do
10     $\tilde{p}_{n+1} \leftarrow p_{n+1} - W p_{n+1}$ 
11     $\tilde{q}_{n+1} \leftarrow q_{n+1} - W^\dagger q_{n+1}$ 
12     $res \leftarrow \min(\|\tilde{p}_{n+1}\|/\|p_{n+1}\|, \|\tilde{q}_{n+1}\|/\|q_{n+1}\|)$ 
13     $p_{n+1}, q_{n+1} \leftarrow \tilde{p}_{n+1}, \tilde{q}_{n+1}$ 
14  end
15   $b_{n+1} \leftarrow \|p_{n+1}\|$  // The argument of  $b_n$  is fixed to be 0.
16   $c_{n+1} \leftarrow q_{n+1}^\dagger p_{n+1}/b_{n+1}$ 
17   $p_{n+1}, q_{n+1} \leftarrow b_{n+1}^{-1} p_{n+1}, c_{n+1}^{-1} q_{n+1}$ 
18 end
19  $a_{d-1} \leftarrow q_{d-1}^\dagger H p_{d-1}$ 

```

KRYLOV WAVE FUNCTIONS

Figure S1 presents several examples of the Krylov wave function for varying W_γ at times $t = 300$ and 1000 , providing additional data depicted in Fig. 1(c) in the main text. Our analysis here corroborates that the wave function exhibits localization around $n \approx 0$ for $W_\gamma < W_L$ ($W_L \approx 0.0351$) on the intermediate time scale ($t = 300$), while delocalization is observed in the long term ($t = 1000$). The apparent flatness of the delocalized wave functions is attributed to the logarithmic scaling of the x -axis, with significant occupation occurring at large n values.

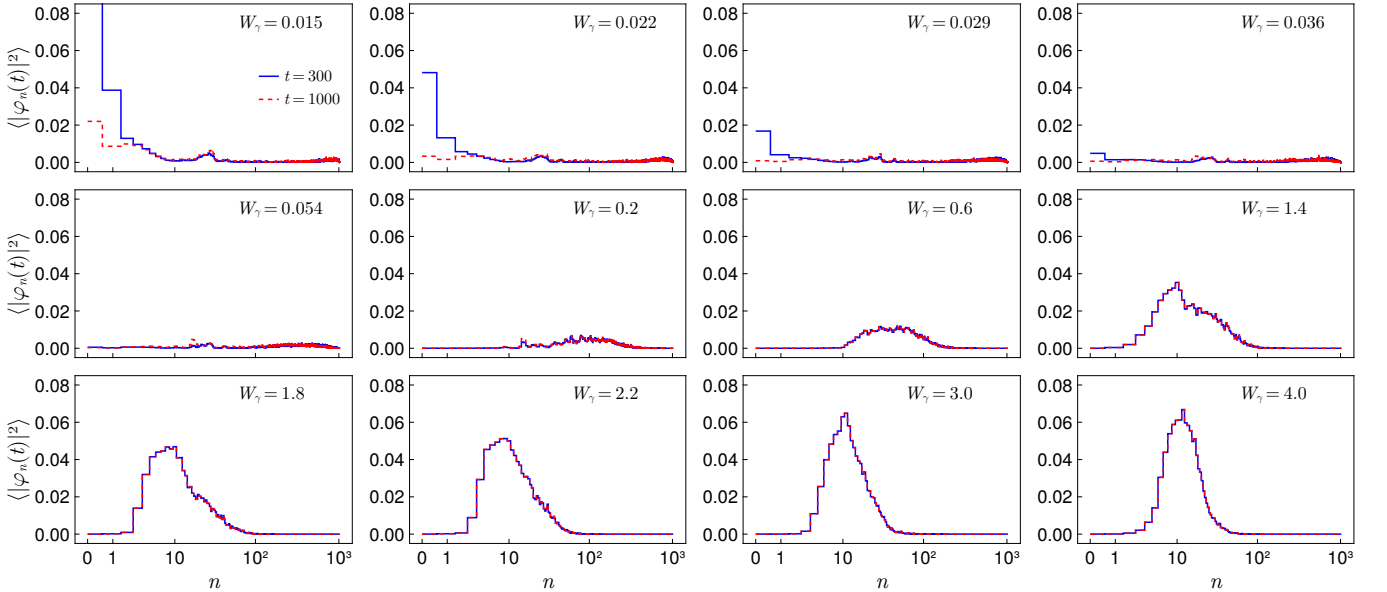


FIG. S1. Krylov wave function at intermediate time $t = 300$ (blue) and long time $t = 1000$ (red) for different W_γ .

When W_γ is comparable or larger than W_L , the Krylov wave function rapidly reaches a steady state characterized by localized features. The difference between the wave functions at $t = 300$ and $t = 1000$ are invisible. It is noted that the central peak shifts to smaller n values as W_γ increases.

When $W_\gamma > W_C$ ($W_C = 1.647$), the saturated Krylov complexity remains relatively constant. The critical behavior may not be directly reflected in the Krylov wave function, however, as elaborated in the main text, it can be inferred from the Lanczos coefficients. We introduce the concept of Krylov reciprocity to identify the critical point, which provides a deeper understanding of the system at the phase transition.

EARLY-TIME COMPLEXITY GROWTH

The early-time growth of the Krylov complexity, C_K , exhibits quadratic behaviors. We fit C_K using the function $C_K(t) = at^2$ for $t < 0.01$, and present the coefficients for different system sizes $L = 4, 6, 8, 10$ and a range of W_γ from 0.01 to 10 in Fig. S2. Our analysis reveals that the coefficient a is proportional to L and exhibits a parabolic relationship with W_γ , approximated as $a \simeq L(1 + 0.33W_\gamma^2)$.

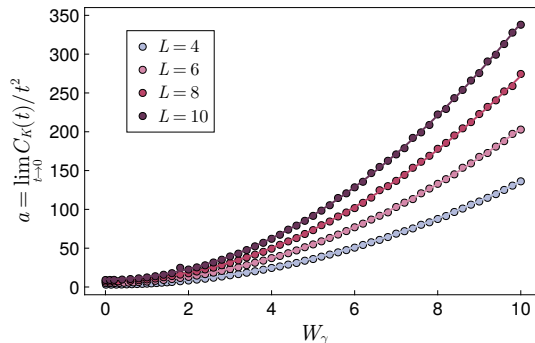


FIG. S2. Early-time growth rate of the Krylov complexity, $a = \lim_{t \rightarrow 0} C_K/t^2$. Solid lines are the fitting with function $a = L(1 + \frac{1}{3}W_\gamma^2)$. The fitting errors are smaller than sizes of the scatters.

FITTING OF LANCZOS COEFFICIENTS WITH TSALLIS q -LOG STATISTICS

Ref. [4] proposes using the Tsallis q -log function to fit the Lanczos coefficients for large n , with $|b_n|^2 \propto -\ln_q(n/2^L)$. The q -log function is defined as

$$\ln_q(x) = \begin{cases} \ln(x) & \text{if } x > 0 \text{ and } q = 1 \\ \frac{x^{1-q} - 1}{1-q} & \text{if } x > 0 \text{ and } q \neq 1. \\ \text{Undefined} & \text{if } x \leq 0 \end{cases} \quad (\text{S9})$$

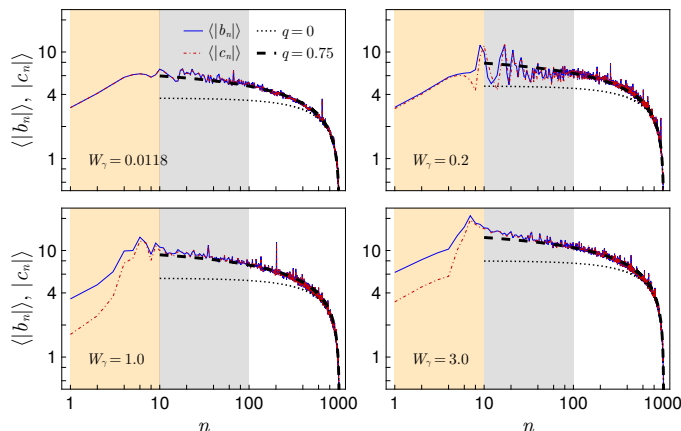


FIG. S3. Fitting of the Lanczos coefficients with Tsallis q -log function.

Thus, the assumption $b_n \propto \sqrt{1 - n/s^L}$ in Ref. [5] can be regarded as a special case with $q = 0$. We fit the average Lanczos coefficients $\langle |b_n| \rangle$ and $\langle |c_n| \rangle$ using the form

$$\langle |b_n| \rangle, \langle |c_n| \rangle \propto \sqrt{1 - (n/2^L)^{1-q}}, \quad (\text{S10})$$

with $q = 0$ and 0.75 , as shown in Fig. S3. We find that $q = 0.75$ provides a better approximation for the values of Lanczos coefficients in the regime where $n > L$, as discussed in the main text.

KRYLOV RECIPROCALITY

In order to show the d -dependence of the Krylov reciprocity, we show the values of $R_K^{(d)}$ for $d = 3$ to 8 in Fig. S4(a1-a6). The crossing behavior is universal for all the choices of d , while their finite-size scaling has some small differences. We find that for $d = 3$ to 7 , the collapsed critical point, W_C , exhibits a plateau, and there is a plateau for $d = 4$ to 6 for the critical exponent, α . Taking the average values for $d = 4$ to 6 , we find that $\langle W_C \rangle = 1.647 \pm 0.014$, and $\langle \alpha \rangle = 0.820 \pm 0.003$. The relative mean deviations are 0.85% and 0.36% for $\langle W_C \rangle$ and $\langle \alpha \rangle$, respectively.

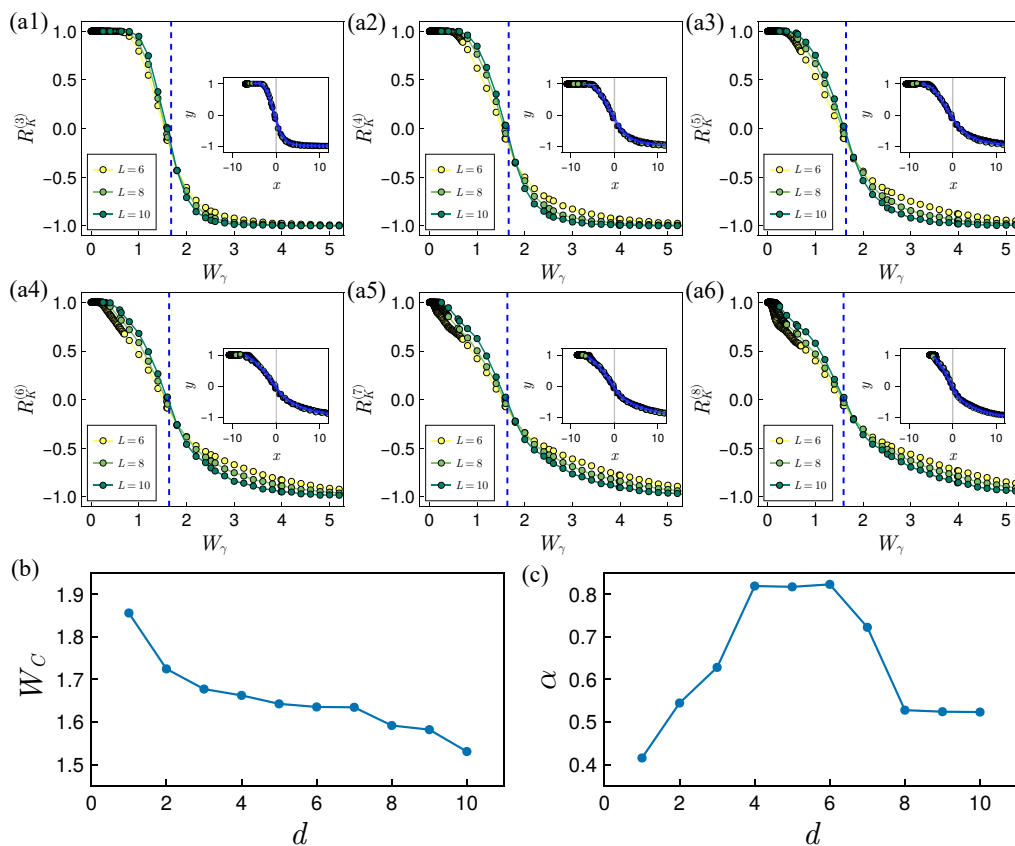


FIG. S4. (a1-a6) Krylov reciprocity $R_K^{(d)}$ for $d = 3$ to 8 . The insets are scaling collapse results for $x = (W_\gamma - W_C)L^\alpha$ and $y = R_K^{(d)}$. The critical points W_C (b) and exponents α (c) are shown to have a shared plateau for $d = 4$ to 6 , which are selected for identification of phase transition.

BIPARTITE ENTANGLEMENT ENTROPY

In this section, we present the bipartite entanglement entropy in Fig. S5. The bipartite entanglement entropy is quantified by the von Neumann entropy of half of the chain, which reads

$$S = -\text{Tr}(\rho_{L/2} \ln \rho_{L/2}), \quad (\text{S11})$$

where the reduced density matrix $\rho_{L/2}$ is derived by tracing out the density matrix of the entire spin chain for sites with indices $j > L/2$.

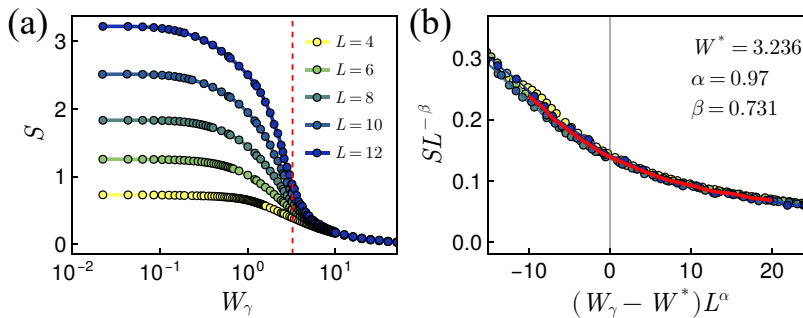


FIG. S5. (a) Bipartite entanglement entropy for varying system size L and non-Hermitian disorder W_γ . The red dashed line gives W^* obtained from the finite-size scaling. (b) Finite-size scaling of S . The Red line is the collapsed universal function by averaging data within the interval for optimization.

In the chaotic regimes where W_γ is small, the entanglement entropy increases in accordance with the volume law, aligning with the observations in Fig. S5(a). At this point, no discernible difference is observed between Hermitian and non-Hermitian chaos, as S approaches constant values when $W_\gamma \rightarrow 0$. As W_γ increases, S tends to diminish, which is consistent with the hypothesis that the system's wave function evolves into product states. Additionally, we have conducted a finite-size scaling analysis, as shown in Fig. S5(b). The critical value W^* as well as the exponents α and β are obtained by minimizing the cosine similarity of the scaled data with the Nelder-Mead algorithm. This method is also applied to other finite-scaling analysis throughout this work. The critical value $W^* = 3.236$ is in proximity to the transition point where the characteristic complex level spacing $\langle r \rangle$ descends to $2/3$, indicative of a 2D Poisson distribution.

Conversely, the examination of the standard deviation of the bipartite entanglement entropy, σ_S , along with Krylov reciprocity, indicates a phase transition at $W_C \approx 1.763$ and 1.647 , respectively, as it departs from the chaotic regime of the AI^\dagger class where $\langle r \rangle_{\text{AI}^\dagger} = 0.7222$.

-
- [1] H. Van Der Veen and K. Vuik, Bi-Lanczos with partial orthogonalization, *Comput. Struct.* **56**, 605 (1995).
 - [2] R. M. Larsen, *Lanczos Bidiagonalization with Partial Reorthogonalization*, Technical Report DAIMI PB-357 (Department of Computer Science, Aarhus University, 1998).
 - [3] J. Liesen and Z. Strakoš, *Krylov Subspace Methods: Principles and Analysis*, 1st ed., Numerical Mathematics and Scientific Computation (Oxford University Press, Oxford, 2013).
 - [4] B. Bhattacharjee and P. Nandy, Krylov fractality and complexity in generic random matrix ensembles, [arXiv:2407.07399](https://arxiv.org/abs/2407.07399) (2024).
 - [5] J. Erdmenger, S.-K. Jian, and Z.-Y. Xian, Universal chaotic dynamics from Krylov space, *J. High Energy Phys.* **2023** (8), 176.